Validation of ASTM F2077 models in Alfonso™: Uniaxial compression of titanium spinal spacers

Non-Confidential Technical Whitepaper – 31 March 2023

Experiments and Analysis: Janice Oentaryo, PhD; Rezaul Tharim; Sloan Kulper, PhD; and Erica Ueda Boles, PhD
Visualizations: Abbas Alvi and Eka Tjong

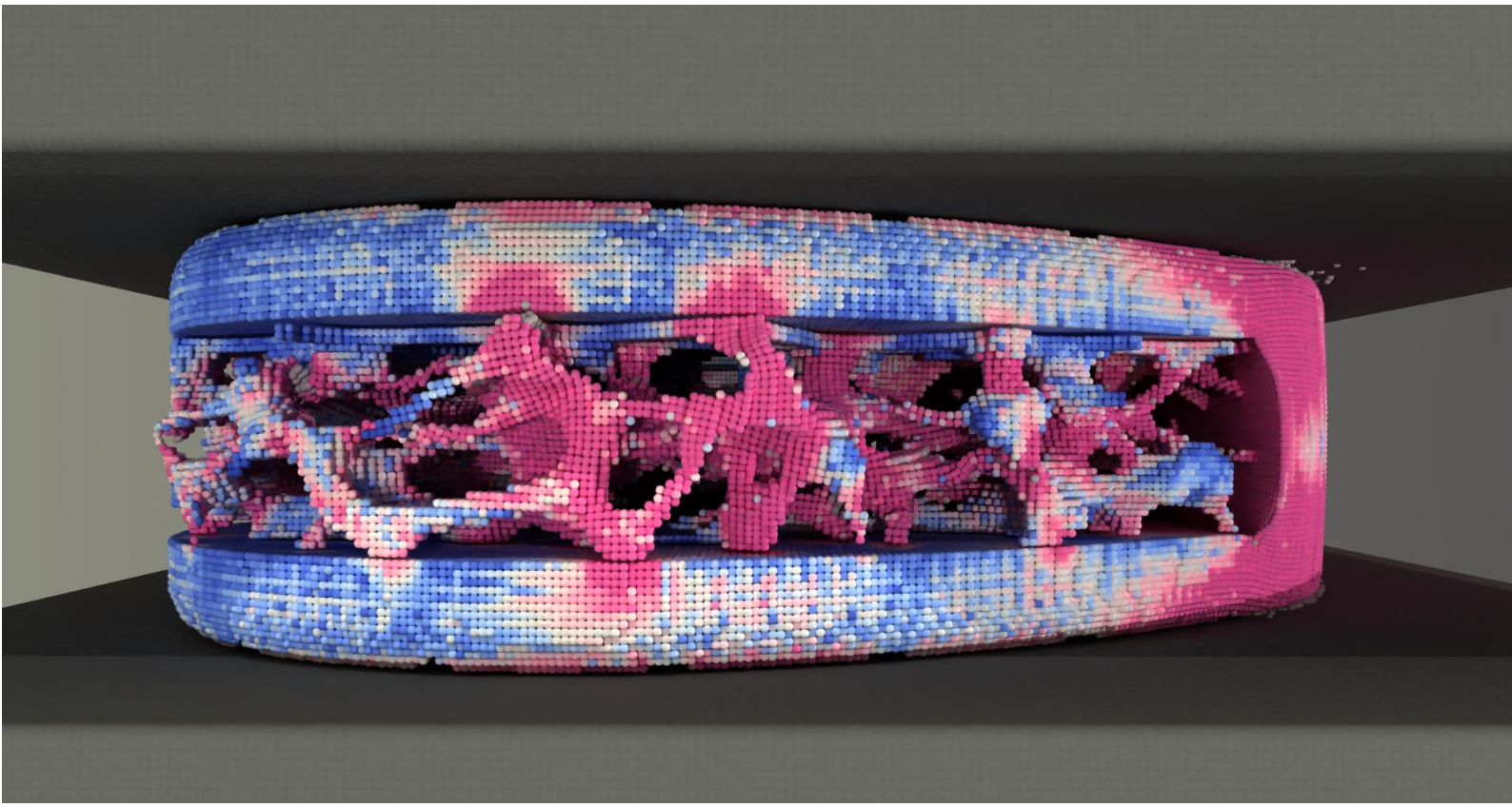

*Simulations were conducted using a commercial, US FDA-cleared intervertebral body spinal fusion device; figure above is of a similar dummy device

Abstract

Computational models of the static axial compression tests of several sizes of additively manufactured Ti-6Al-4V ELI (e.g., material per ASTM F3001-14-2021) lumbar intervertebral body fusion devices were tested using the *Alfonso*™ particle-based simulation system and validated via comparison to experimental data. Commercially available US FDA-cleared 3D-printed titanium devices of two different sizes (H13 and H11 mm; n=5 specimens for each group) were tested by an independent laboratory according to the ASTM F2077-22 standard. Devices were axially compressed at a loading rate of 2 mm/min until functional failure or until the maximum load capacity of the test frame was reached. Prior to testing, micro-CT scans were collected for each specimen at a resolution of 182 µm/pixel and then converted to particle models in *Alfonso*™ for simulated ASTM F2077-22 static axial compression, using a material model based on the typical properties of Ti-6Al-4V ELI. The average stiffness value of the device (K_d) for the H13 mm device was 15,602 and 16,944 N/mm in the physical and simulated test, respectively. The average K_d value for the H11 mm device was 26,325 and 30,791 N/mm in the physical and simulated tests, respectively. The average CCC (concordance correlation coefficient) between the force–displacement curves for the simulation and experiment was >0.85, suggesting excellent concordance. *Alfonso*™ can accurately predict the stiffness of various compliant porous 3D-printed titanium intervertebral body fusion devices based on implant geometry and standard material properties.

Background and objectives

ASTM F2077-22 is a standard test method used to evaluate the performance of non-biologic intervertebral body fusion devices (e.g., under FDA product code MAX, 21 CFR §888.3080) designed to promote arthrodesis or fusion at a given spinal motion segment. It is typically part of a battery of tests required to demonstrate that a study device is substantially equivalent to a legally marketed predicate device in a 510(k) premarket submission. Alfonso's particle-based model of ASTM F2077-22 can be used to quickly predict the likelihood that a candidate design will perform sufficiently without needing to produce and test a physical prototype. To validate Alfonso's predictions, we compared the load displacement curves of simulated and physical static axial compression tests of different sizes of porous 3D-printed titanium-6 aluminum-4 vanadium extra low interstitials (Ti-6Al-4V ELI) transforaminal lumbar interbody fusion (TLIF) devices.

Materials and methods

Preparation and testing of physical specimens

Two different sizes of commercial, US FDA-cleared bullet banana-shaped, 3D-printed porous Ti-6Al-4V ELI (e.g., ASTM F3001 material specification) TLIF devices underwent physical mechanical F2077-22 static axial compression tests (n=5 samples of each device size, dimensions are summarized in Table 1). Intervertebral body fusion devices made out of titanium alloys are conventionally used due to their durability and strength, biocompatibility, corrosion-resistance, and higher osteoconductive potential that leads to optimum fusion rates.[1] These device designs were chosen for initial validation because they cover a common range of dimensions with a generic shape that is commonly used clinically and are offered by various manufacturers. Material properties for the Ti-6Al-4V ELI (Grade 23) as summarized from manufacturers' sources are listed in Table 2.[2]–[4]

Table 1. Design specifications of the two different sizes of bullet banana-shaped Ti-6Al-4V ELI TLIF devices

Dimensions	Ti-6Al-4V ELI TLIF device	
	Large (H13 mm)	Medium (H11 mm)
Height (mm)	13	11
Lordosis angle (°)	8	8
Length (mm)	32	28
Width (mm)	10	10
Number of specimens	5	5

Physical ASTM F2077-22 static axial compression testing was performed by an independent certified testing laboratory using the test setup illustrated in Figure 1. For all device sizes, conformal superior and inferior test fixture blocks of stainless steel were manufactured with a pocket depth of 1 mm at the deepest point. After placing each device between the corresponding pair of test blocks, compressive load was applied with a hydraulic test frame at a rate of 2 mm/min until functional failure or until the maximum load capacity of the test frame was reached.

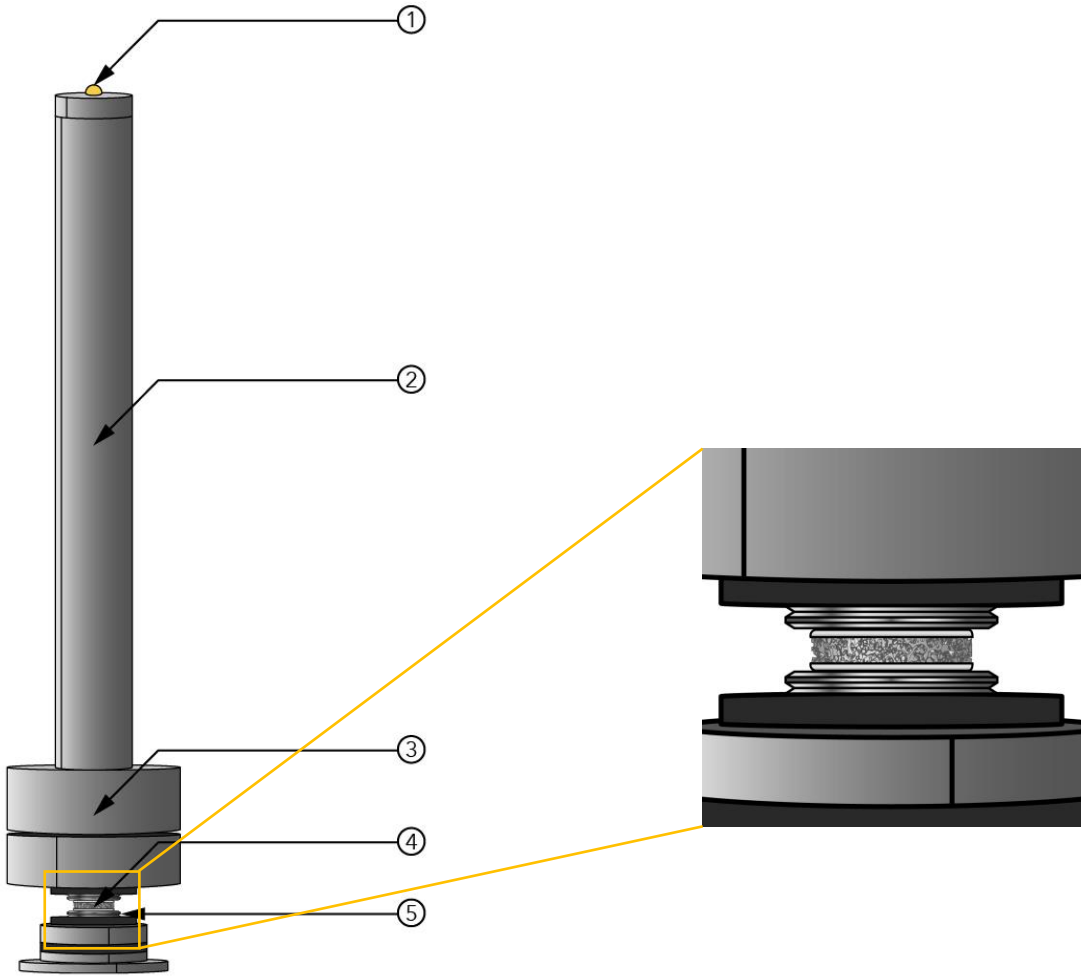

Figure 1. Physical test setup: 1. Ball and socket bearing, 2. Metal pushrod, 3. Spherical bearing, 4. Implant, 5. Steel test block. Illustration by Eka Tjong

Preparation and testing of simulated specimens

Prior to the physical tests, all spinal spacers were scanned by micro-CT at a resolution of 182 µm/pixel (Bruker Skyscan 1076, Bruker Corporation). The DICOM image stacks underwent 3D registration and were converted to particle models of the implant geometry using standard material properties for Ti-6Al-4V ELI as summarized in Table 2 (see "Appendix I: Notes on particle-based methods in *Alfonso*" for further details). Each implant particle model was sandwiched between two simulated conformal rigid testing blocks, with similar dimensions and pocket geometry as the physical testing blocks (see Figure 2).

A sensitivity analysis was conducted to determine the maximum uniaxial compression rate (5 m/s), below which there was no observable change in the force–displacement curve. This rate was also much less than the calculated speed of sound of the implant material (Table 2). Simulated axial compression tests were then performed at this rate for all samples. Deviations between the physical and simulated testing protocols and the published ASTM F2077-22 standard are summarized in Table 3. Note that models in *Alfonso*™ do not typically simulate the strain-rate dependent viscoelastic behaviors of materials for static tests; as physical static benchtop tests are usually conducted at very low rates of motion, we consider strain-rate components to be negligible.

The speed of sound c was calculated to set a theoretical upper bound for the rate of motion of the simulation (Table 2):

$$c = \sqrt{\frac{(K_f + \frac{4}{3}G_f)}{\rho}}$$

Where K_f is the bulk modulus, G_f is the shear modulus, and ρ is the density (kg/m^3) of the material.

Table 2. Typical material properties of Ti-6Al-4V ELI from manufacturers' datasheets [2]–[4]

Typical material properties	Ti-6Al-4V ELI (Grade 23)
Density (kg/m^3)	4428.78
Elastic Modulus (GPa)	104.80
Poisson's Ratio	0.342
0.2% Yield Strength (MPa)	827
Ultimate Tensile Strength (MPa)	896
Elongation at break (%)	15
Reduction of Area (%)	45
Speed of sound $\mathbf{c}$ (m/s)	6059

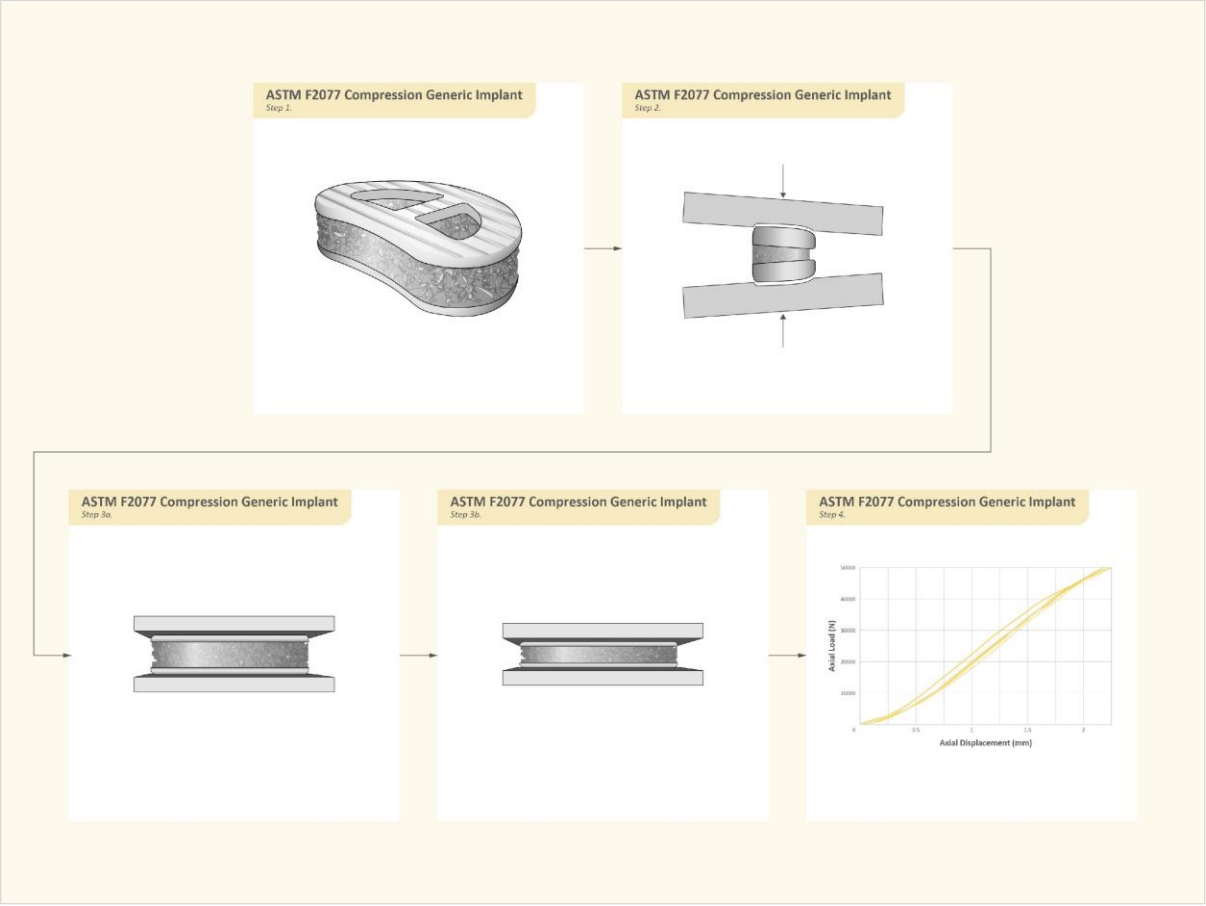

Figure 2. Illustration of the overall ASTM F2077-22 static axial compression test simulation procedure in Alfonso™ Illustration by Eka Tjong

Table 3. Deviations between physical and simulated testing protocols and the published ASTM F2077-22 standard

Test Setup Procedures / Parameters		ASTM F2077-22 Static axial compression standard method	Physical test	Simulation
Test setup procedures	Load fixture	(1) Ball and socket joint; (2) Stainless-steel hollow pushrod D25 mm with one 25 mm radius concave spherical end, and other end having ball and socket joint. The length of the pushrod between the center of the ball-and-socket joint to the center of the spherical surface is to be a minimum of 38 cm; (3) Superior fixture with stainless steel sphere's diameter of at least 50 mm truncated to locate center at geometric center of intervertebral device	Follows the ASTM F2077-22 standard	Load fixture was not simulated. For the devices with lordosis angle (e.g., 8° angle in H11 mm and H 13mm study devices), the virtual superior and inferior test blocks were angled +4° and –4° above and below the horizontal plane, respectively, to mimic the degree of lordosis angle.
	Load application	The actuator of the testing machine is connected to the pushrod by a minimal friction ball-and-socket joint or universal joint (that is, unconstrained in bending). The pushrod is connected to the superior fixture by a minimal friction sphere joint (that is, unconstrained in bending and torsion). The hollow pushrod should be of minimal weight to be considered as a "two-force" member. It thus applies to the intervertebral body fusion device assembly a resultant force directed along the pushrod's axis and located at the center of the superior fixture's sphere joint (the geometric center of the device being tested).	Follows the ASTM F2077-22 standard	The virtual superior metal block axially compressed the device at a specified rate of displacement. The joints were not modeled in these simulations.

Test Setup Procedures / Parameters		ASTM F2077-22 Static axial compression standard method	Physical test	Simulation
	Metal block	Two metal blocks as superior and inferior fixtures. The blocks are to have surfaces that mate geometrically within the intervertebral device similar to how the device is intended to mate with vertebral end plates. The metal blocks may be reused if undamaged.	Two stainless steel blocks as superior and inferior fixtures. For each device size, the pocket for each metal block was manufactured using a 0.5 mm milling cutter to match the cage's outer geometry and to have a pocket depth of 1 mm at the deepest point. The same metal blocks were used for all specimens of the same size.	Two virtual rigid metal blocks as superior and inferior fixtures. For each device size, two virtual metal blocks were generated with the pockets matching the cage's outer geometry with a maximum pocket depth of 1 mm (same as the physical test blocks). The same virtual metal blocks were used across all specimens of the same size.
	Initial intradiscal height	Shall be constant for all tests for an intervertebral body fusion device assembly of a given size.	11 mm for H13 mm spacer and 9 mm for H11 mm spacer	Same as the physical test
	Sample size	Usually, n=5 minimum per case	n=5 per group	n=5 per group
Parameters	Axial compression rate	No greater than 25 mm/min	2 mm/min	5 m/s
	Data collection time interval	Not mentioned; suitable to continuously record load versus load fixture displacement	0.02 s	1×10^{-9} s
	Type of data	Load–displacement data, which will be used to calculate the yield displacement (mm), stiffness (N/mm), yield load (N), ultimate displacement (mm), and ultimate load (N).	Follows the ASTM F2077-22 standard	Follows the ASTM F2077-22 standard
	End point	The load–displacement data is generated until functional or mechanical failure of the intervertebral body fusion device assembly is obtained.	Follows the ASTM F2077-22 standard or until the maximum load capacity of the test machine was reached	Up to the maximum displacement as compared to the physical data; The load–displacement data is generated until functional or mechanical failure of the intervertebral body fusion device assembly is obtained.
	Resolution (specific to simulation)	Not applicable	Not applicable	182 µm

Data and statistical analyses

The load–displacement data were normalized such that zero displacement was set at the lowest initial force common for both the physical data and the *Alfonso*™ simulation data. The displacements for all simulation data were offset by 0.25 mm to compensate for the initial "toe-in" region seen on the graphs for the physical data, which is likely due to adjustment in position and settling of the joint fixtures upon initial loading in the physical test. Due to the 50 kN limits of testing frame used by the independent laboratory, they could not determine the yield load, yield displacement, ultimate load, and ultimate displacement of the physical specimens. Therefore, in this whitepaper, we focus on comparing the stiffness value of the devices determined from the physical and simulation data, as this is a necessary input for ASTM F2267-22 subsidence test calculations. Stiffness in the initial linear-elastic region of both the physical and simulation data was calculated in the load range from 8,000 N to 18,000 N.

To serve as additional quantitative analysis on the load–displacement graphs, concordance analyses were performed across the load–displacement curves to examine the extent of similarity. The numbers of data points obtained from the physical tests and *Alfonso*™ simulations varied due to the difference in data collection intervals. To directly compare and analyse the load–displacement data for the concordance analysis, Python scripts were used to resample the data sets to the same displacement values and interpolate the load values without changing the load–displacement curves' shape and magnitude. Statistical analyses were performed using MedCalc® (MedCalc Software Ltd, Ostend, Belgium).

Note: Lin's concordance correlation coefficient (CCC)

Lin's concordance correlation coefficient (CCC) evaluates the degree to which pairs of observations fall on the 45° line through the origin (i.e., the line of equality). [2], [3] The concordance correlation coefficient is calculated as $\rho_c = \rho \times C_b$ ($-1 \leq \rho_c \leq 1$) where:

- ρ is the Pearson correlation coefficient, which measures how far each observation deviates from the best-fit line, and is a measure of precision, and
- C_b is a bias correction factor that measures how far the best-fit line deviates from the 45° line through the origin and is a measure of accuracy ($0 < C_b \leq 1$; $C_b = 1$ when there is no deviation from the 45° line).

A CCC value of 1 indicates strong concordance, while a value of -1 indicates strong discordance. Borrowing from the standard interpretation of Pearson's correlation coefficient or intraclass correlation coefficients, we assume that positive CCC values <0.20 indicate "poor" concordance, while values >0.80 indicate "excellent" concordance.

Results

After undergoing static axial compression, either physical or simulated, all samples underwent functional failure. As described by ASTM F2077-22, implant functional failure is described as permanent deformation that results in the intervertebral body fusion device assembly to be ineffective or unable to resist force and/or adequately maintain attachment. The plastic deformation observed in the simulation is represented by the stress and material failure of a dummy device that underwent static axial compression as shown in Figure 3.

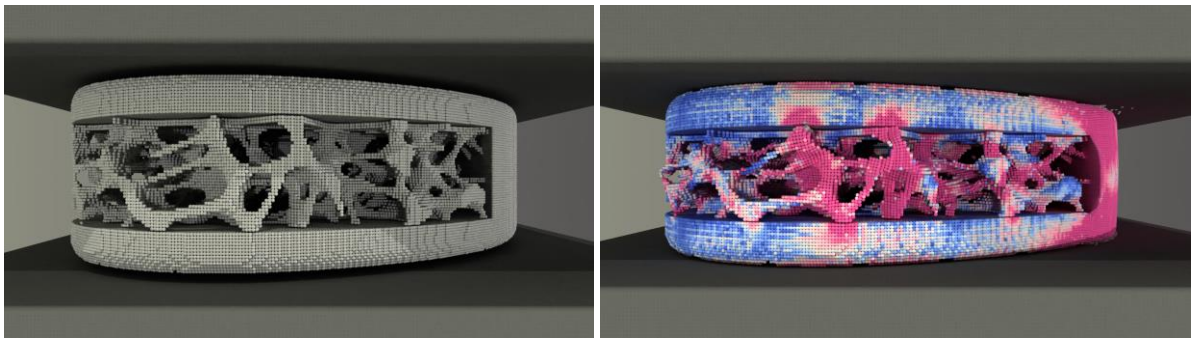

Figure 3. Representative images showing a simulated ASTM F2077-22 static axial compression test with a similar dummy device, whereas the actual simulations were conducted using a commercial, US FDA-cleared intervertebral body fusion device.

The average CCC between the load–displacement curves of the physical and simulated tests across all implant sizes was 0.88 (using more than 100 sample points per curve, see Table 4), suggesting excellent concordance.

For the large-sized H13 mm device, the overall load–displacement curves were comparable between the physical and simulation data (see Figure 4); the average K_d values were 15,602 and 16,944 N/mm in the H13 mm physical and simulated tests, respectively (see Table 4). However, it is noted that the physical load–displacement curve for specimen 4 for the H13 mm device had a dissimilar curve shape compared to the other trials and resulted in a lower stiffness value. The external testing lab had reported that based on the permanent impression caused by the load block on the top surface of this specimen; it is suspected that specimen 4 slipped out of the pocket during the physical test. The average CCC between the load–displacement curves of the H13 mm device in the physical and simulated test pairs was 0.87.

For the medium-sized H11 mm device, the overall physical and simulation load–displacement curves were similar, especially in the yield regions (see Figure 5); the average K_d values were 26,325 and 30,791 N/mm in the H11 physical and simulated tests, respectively (see Table 4). The average CCC between the load–displacement curves of the H11 mm device in physical and simulated test pairs was 0.89.

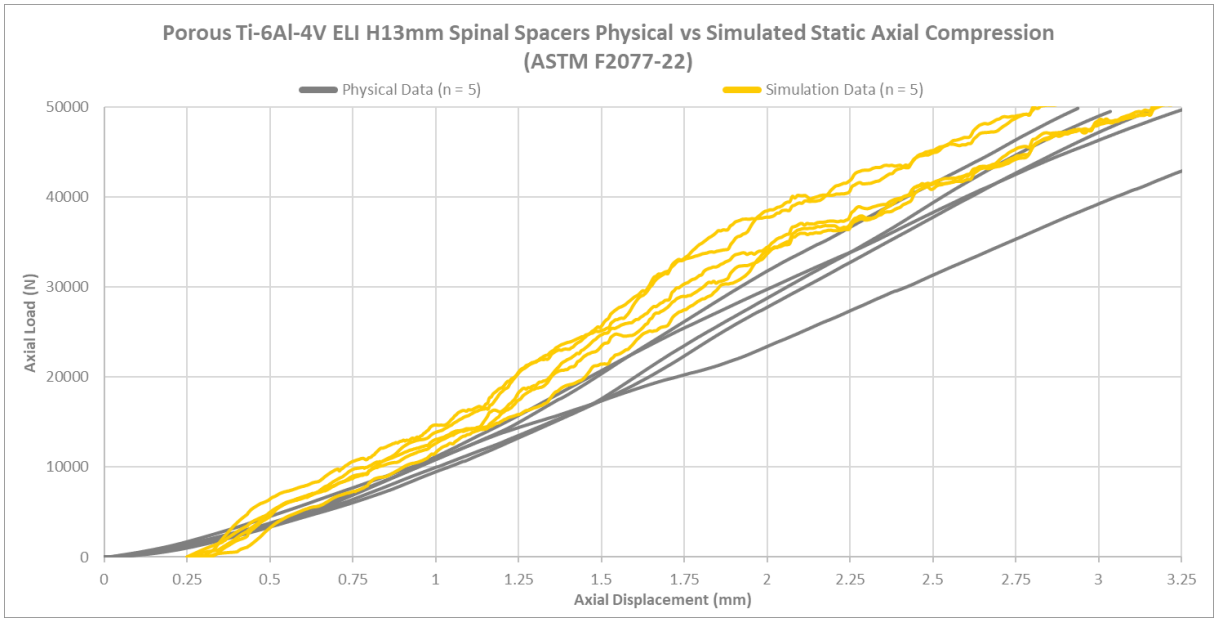

Figure 4. Load-displacement curves from the physical experiment (n = 5) and the simulated (n = 5) static axial compression tests of large-sized H13 mm porous Ti-6Al-4V ELI spinal spacers

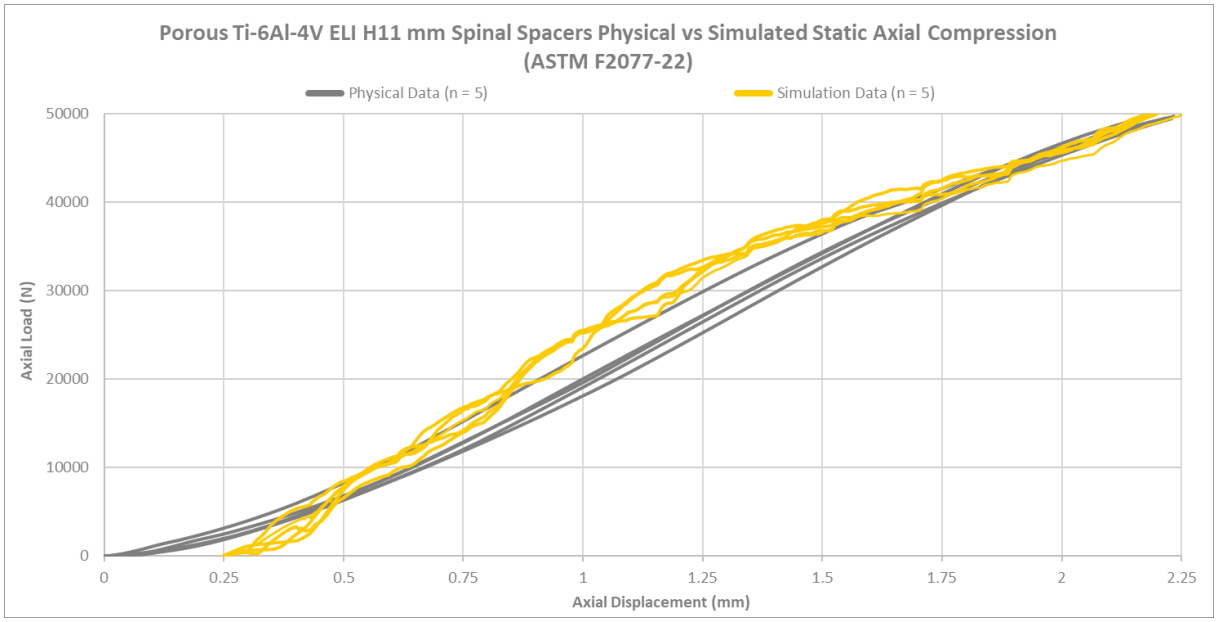

Figure 5. Load-displacement curves from the physical experiment (n = 5) and the simulated (n = 5) static axial compression tests of medium-sized H11 mm porous Ti-6Al-4V ELI spinal spacers

Table 4. Calculated values of the device's stiffness (K_d) from ASTM F2077-22 static axial compression tests

Specimens	Physical vs Simulation Data for Stiffness of the Device (K_d, N/mm)			
	H13 mm, 8°, 32x10mm Spinal Spacer		H11 mm, 8°, 28x10mm Spinal Spacer	
	Physical	Simulation	Physical	Simulation
Specimen 1	17,138	16,786	28,502	31,850
Specimen 2	15,738	19,802	26,913	30,964
Specimen 3	14,763	15,895	23,954	29,389
Specimen 4	13,495 *	17,099	26,214	25,443
Specimen 5	16,879	15,138	26,044	36,309
Average	15,602	16,944	26,325	30,791
Standard Deviation	1,512	1,773	1,643	3,942

* The external testing lab had reported that based on the permanent impression caused by the load block on the top surface of specimen 4; it is suspected that this sample slipped out of the pocket during the test.

Table 5. Concordance analysis of the device's stiffness (K_d) from ASTM F2077-22 static axial compression tests

Variables	H13 mm, 8°, 32x10mm Spinal Spacer				
	Physical Data 1 vs Simulation Data 1	Physical Data 2 vs Simulation Data 2	Physical Data 3 vs Simulation Data 3	Physical Data 4* vs Simulation Data 4	Physical Data 5 vs Simulation Data 5
Sample size (curve data points)	163	159	152	175	147
Concordance correlation Coefficient (CCC)	0.8572	0.8271	0.9030	0.8259	0.9236
95% Confidence Interval	0.8256 to 0.8834	0.7884 to 0.8593	0.8773 to 0.9235	0.7917 to 0.8549	0.9020 to 0.9406
Pearson ρ (precision)	0.9870	0.9759	0.9816	0.9889	0.9835
Bias correction factor C_b (accuracy)	0.8684	0.8476	0.9199	0.8351	0.9391
Variables	H11 mm, 8°, 28x10mm Spinal Spacer				
	Physical Data 1 vs Simulation Data 1	Physical Data 2 vs Simulation Data 2	Physical Data 3 vs Simulation Data 3	Physical Data 4 vs Simulation Data 4	Physical Data 5 vs Simulation Data 5
Sample size (curve data points)	112	106	107	111	109
Concordance correlation coefficient (CCC)	0.9069	0.9035	0.8797	0.8915	0.8860
95% Confidence Interval	0.8783 to 0.9290	0.8709 to 0.9282	0.8410 to 0.9095	0.8581 to 0.9174	0.8501 to 0.9137
Pearson ρ (precision)	0.9864	0.9766	0.9724	0.9816	0.9772
Bias correction factor C_b (accuracy)	0.9193	0.9252	0.9047	0.9082	0.9066

* The external testing lab had reported that based on the permanent impression caused by the load block on the top surface of specimen 4, it is suspected that this sample slipped out of the pocket during the test.

Conclusion

This validation study suggests that *Alfonso*™ can accurately predict the compliance of 3D-printed porous Ti-6Al-4V ELI intervertebral body fusion devices in different sizes (e.g., H13 and H11 mm) during axial compression, providing supplementary data or replacing certain physical testing according to ASTM F2077-22 "Test Methods for Intervertebral Body Fusion Devices." The measurement outputs from the *Alfonso*™ simulations of the static axial compression tests follow the ASTM F2077-22 test standard, namely the load–displacement curve from which we can calculate the stiffness of the device, yield load, yield displacement, ultimate load, and ultimate displacement. The physical and simulated static axial compression tests of this study resulted in load–displacement curves with excellent concordance as well as agreement between the slopes of the linear-elastic regions. Beyond the outputs of a physical test, *Alfonso*™ can also provide 3D visualizations of material failure (e.g., plastic deformation, cracking - as stress and strain field data - throughout the entire device during compression. Taken together, this study suggests that *Alfonso*™ can serve as an excellent non-clinical assessment tool in support of pre-regulatory deliberations and regulatory submissions for intervertebral body fusion devices.

References

[1] C. D. Ray, "Threaded titanium cages for lumbar interbody fusions," *Spine (Phila Pa 1976)*, vol. 22, no. 6, pp. 667–669, Mar. 1997.

[2] MatWeb, " Titanium Ti-6Al-4V ELI (Grade 23), Annealed," 2023.

[3] AZO Materials, "Grade 23 Ti 6Al 4V ELI Alloy (UNS R56401)," 2013.

[4] Carpenter Technology, "Ti 6Al-4V ELI," Sep. 2021.

Appendix I

Notes on particle-based method simulation in *Alfonso*™

- "Resolution" (e.g., 50, 200, 500 µm) in *Alfonso*™ is typically equivalent to the diameter of the particles in the model, and thereby the minimum distance within which particles begin to interact. The degree of interaction between particles varies continuously as a function of their distance (e.g., in compression, particles repel more vigorously the closer they are to one another, while the reverse is true for tensile forces acting between "bonded" particles of the same object).
- Each particle represents a small volume of mass of an object in the analysis, the material properties of which (elastic modulus, yield, failure, hardening criteria, etc.) dictate the responses of particles to forces applied during analysis.
- Micro-CT scans of the physical intervertebral body fusion devices were collected and reconstructed. For the post-processing steps, the micro-CT scans underwent 3D-registration for alignment ensuring the samples were in similar positions for the simulation setup. The scans were converted to point files upon applying a suitable thresholding value and selection of the region of interest.
- Using the stated material properties from the manufacturer as a starting point, a proprietary scaling factor of the failure mean and standard deviation was applied uniformly to the ultimate strength of Ti-6Al-4V ELI.
- In general, we do not scale material density (i.e., mass) in *Alfonso*™.
- While the initial positions of particles are typically spaced in discrete increments of the resolution (e.g., 182 µm in this particular validation study), during analysis particles may continuously move in 3D space. For instance, a particle initially at (182, 182, 182) may move to (182.0034, 181.793403, 184.09809823462) during analysis.
- "Bonds" between particles in *Alfonso*™ are typically formed only at the initial time state, and then only between neighboring particles of the same object. Bonded particles resist both compression and tension, per the homogeneous or heterogenous properties of the material, until the stress or strain failure limits of the material are exceeded, and a crack is formed. Failed particles remain in analysis (e.g., as debris) and continue to interact with other particles, allowing phenomena such as compaction to be faithfully reproduced in *Alfonso*™.
- "Unbonded" particles that come into contact after analysis has begun (i.e., particles that move to within the minimum distance of interaction) will not form bonds and will only repel one another.
- (See "Beyond FEA: Particle-based simulation 101" at https://www.lifespans.net/publications for further discussion of the basics of mesh-free analysis)